Item 830-H-15 NAS 1.60:1007

JAN 30 1978

NASA Technical Paper 1007
DOE Report CONS/1011-12
Joint Program with the
Department of Energy

COMPLETED
ORIGINAL

Cold-Air Performance of Free-Power Turbine Designed for 112-Kilowatt Automotive Gas-Turbine Engine

I - Design Stator-Vane-Chord Setting Angle of 35°

Milton G. Kofskey and William J. Nusbaum

JANUARY 1978

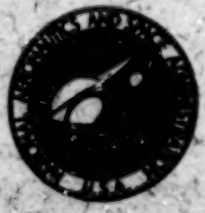

24

NAS 1.60:1007

NASA Technical Paper 1007
DOE Report CONS/1011-12
Joint Program with the
Department of Energy

Cold-Air Performance of Free-Power Turbine Designed for 112-Kilowatt Automotive Gas-Turbine Engine

I - Design Stator-Vane-Chord Setting Angle of 35°

Milton G. Kofskey and William J. Nusbaum
Lewis Research Center
Cleveland, Ohio

National Aeronautics
and Space Administration

Scientific and Technical
Information Office

1978

COLD-AIR PERFORMANCE OF FREE-POWER TURBINE DESIGNED FOR 112-KILOWATT AUTOMOTIVE GAS-TURBINE ENGINE I - DESIGN STATOR-VANE-CHORD SETTING ANGLE OF 35°

by Milton G. Kofskey and William J. Nusbaum

Lewis Research Center

SUMMARY

An experimental investigation of the baseline-power turbine designed for a 112-kilowatt automotive gas-turbine engine was made to determine its performance over a range of speed and pressure ratio at the design power-point setting of the variable stator.

An equivalent mass flow of 1.014 kilograms per second was obtained at design equivalent speed and design equivalent overall pressure ratio of 1.698. This value of mass flow is about 5.7 percent smaller than design value of 1.075. This is partially the result of a smaller turbine flow area resulting from operation of the turbine at a lower than design gas temperature. Thermal expansion of the turbine when operated at the design inlet temperature would increase the flow area and consequently the equivalent mass flow by about 2 percent.

The total efficiency based on conditions obtained at the stator inlet and rotor exit was slightly above 0.77 at design equivalent speed and design equivalent power. The static efficiency for the same operating point was slightly above 0.70.

The total and static efficiency based on conditions obtained at the stator inlet and exit collector was slightly over 0.76 at design equivalent speed and design equivalent power. The efficiencies indicate that there was about a 1-point drop in total efficiency and a 6-point rise in static pressure through the diffuser and exit collector. The diffuser and exit collector recovered 85.7 percent of the rotor-exit kinetic energy.

The overall static-pressure-recovery coefficient of the diffuser was 0.28, and the static-pressure recovery of the diffuser was about 52 percent of that recovered by the diffuser and exit collector. The diffuser effectiveness was 0.36. The diffuser effectiveness could be increased to 0.76 if the diffuser average-surface-length-to-inlet-annulus-height ratio was increased to 5.0 from the present value of 3.13. This would result in about a 3-point increase in static efficiency over the present value of 0.725 based on stator-inlet to diffuser-exit conditions. This improvement in efficiency may not be reflected in a significant increase in overall efficiency based on stator-inlet to exit-collector conditions.

INTRODUCTION

The Department of Energy (formerly the Energy Research and Development Administration) is conducting a program to demonstrate a gas-turbine-powered automobile that meets the 1978 Federal Emissions Standards with acceleration characteristics and fuel economy that are competitive with current conventionally powered vehicles.

One part of the program involves the performance evaluation of a sixth generation gas-turbine engine which was designed and fabricated (ref. 1) by the Chrysler Corporation. This engine delivers 112 kilowatts in a 2000-kilogram vehicle.

The Lewis Research Center, under an interagency agreement, was given the responsibility for evaluating the performance of the Chrysler gas-turbine engine. This engine was to be used as a baseline for the development of an upgraded automotive gas-turbine engine. Accordingly, engine tests as well as cold-air component tests of the turbomachinery are being made. Results of tests to determine the overall external heat loss from the engine are given in reference 2.

This report describes the cold-air performance characteristics of the free-power turbine, which uses a variable stator for engine control and braking. Performance was determined for a stator-vane-chord setting angle of 35° from the plane of rotation. This is the design setting angle for the 100-percent power condition. Tests were made with an inlet pressure of about 0.42 bar and an inlet total temperature of about 303 K. These conditions give a Reynolds number that is equal to that at actual hot-engine operating conditions. Data were obtained over a range of speed from 0 to 130 percent of design and pressure ratio from 1.11 to 2.45.

This report describes the turbine and its performance with and without the exit diffuser. Results are expressed in terms of power, torque, mass flow, and efficiency. The results of radial surveys of rotor-exit flow angle and total pressure at design equivalent speed and design equivalent power are included.

SYMBOLS

A	flow area, cm^2	P	power, kW
AR	aspect ratio, b/c	p	absolute pressure, bar
b	blade height, cm	R_x	blade reaction, $\left(W_4^2 - W_3^2\right)/2U\,\Delta V_u$
c	blade chord, cm	r	radius, cm
e	diffuser overall effectiveness	s	blade spacing or pitch, cm
Δh	specific work, J/g	T	temperature, K

U	blade velocity, m/sec
V	absolute gas velocity, m/sec
W	relative gas velocity, m/sec
w	mass flow, kg/sec
α	absolute gas-flow angle measured from axial direction, deg
β	relative gas-flow angle measured from axial direction, deg
γ	ratio of specific heats
δ	ratio of inlet total pressure to U.S. standard sea-level pressure, P_2'/P^*
ϵ	$= \frac{0.740}{\gamma}\left(\frac{\gamma+1}{2}\right)^{\gamma/(\gamma-1)}$
η	turbine efficiency
θ_{cr}	$= (V_{cr}/V_{cr}^*)^2$
σ	solidity, c/s
τ	torque, N-m
ω	turbine speed, rad/sec

Subscripts:

cr	condition corresponding to Mach number of unity
eq	equivalent
i	ideal
t	tip
u	tangential component
1	station upstream of prerotation vane (fig. 5(a))
2	stator-inlet station (fig. 5(a))
3	stator-exit station (fig. 5(a))
4	rotor-exit station (fig. 5(a))
5	station just inside diffuser exit (fig. 5(a))
6	exit-collector station (fig. 5(a))

Superscripts:

'	absolute
*	U.S. standard sea-level conditions (temperature 288.15 K; pressure, 1.02 bar)

TURBINE DESCRIPTION

The free-power automotive turbine was designed to deliver 112 kilowatts in a 2000-kilogram vehicle. The design-point parameters are listed in table I for engine operating conditions and air equivalent conditions. Air equivalent values for the design-point parameters correspond to operation at U.S. standard sea-level conditions.

Figure 1 is a schematic of the power turbine as set up for tests. Engine components such as the interstage duct, variable stator, rotor, exit diffuser, and bearing assembly were used to build the test rig.

Stator Vanes

A variable stator was designed to provide engine braking and control. Since this requires that the vanes rotate through large arcs, the stator assembly was designed with concentric spherical end walls. The pivot axis of the variable stator was chosen to be on a radial line passing through the center of the concentric spheres. This design allows rotation through the entire operating range of stator setting angles with no change in vane end clearances. The measured vane end clearances were 0.041 and 0.025 centimeter at the inner and outer walls, respectively, which amount to 1.9 and 1.1 percent of the vane height at the inner and outer walls, respectively. The stator assembly (fig. 2) consists of 27 vanes. The stator vanes have changing cross sections and twist from hub to tip. The stator has an aspect ratio of 0.839. The salient stator aerodynamic parameters are given in table II. The stator pivot shank was modified to minimize air leakage from the stator passage to the exit collector along the vane shank by installing an O-ring on the pivot shank. The air leakage through the shank was minimized for two reasons. First, the results are presented in terms of blading or aerodynamic efficiency, which does not include losses due to friction of bearings and seals nor any loss due to leakage along the blade shank. Second, losses resulting from this leakage would have a larger effect on performance in the cold-air performance tests than actual operation in the engine at the higher pressure and temperature levels. The design vane chord setting angle was 35° from the plane of rotation at the mean blade height. This angle corresponds to a vane-exit mean camber line angle of about 67° as measured from the axial direction.

Rotor Blades

The rotor has 51 blades and an aspect ratio of 1.486, based on the mean blade height and the mean section actual blade chord. The rotor has a constant hub diameter that increases from a value of 18.753 to 18.966 centimeters through the blade row. The radial tip clearance was 0.046 centimeter, which is about 2 percent of the annular passage height. The rotor blades also have a changing cross section and twist from hub to tip. A photograph of the rotor is shown in figure 3, and the main aerodynamic parameters are listed in table II.

APPARATUS, INSTRUMENTATION, AND PROCEDURE

Apparatus

The apparatus consisted of the turbine, an airbrake dynamometer to absorb and measure the power output of the turbine, and an inlet and exhaust piping system with flow controls. (See fig. 4.) Pressurized dry air was used as the driving fluid for the turbine.

The air was piped into the turbine through a filter, a mass-flow measuring station consisting of a calibrated flat-plate orifice, and a remotely controlled pressure-regulating valve. The air, after passing through the turbine, was exhausted through a system of piping and a remotely operated valve into the laboratory low-pressure exhaust system.

A row of prerotation vanes was installed in the inlet section of the interstage duct (fig. 1) to simulate the whirl that would be imparted to the air by the compressor-drive turbine in the engine.

The airbrake dynamometer was cradle mounted on air bearings for torque measurement. The force on the torque arm was measured with a commercial strain-gage load cell. The rotational speed was measured with a magnetic pickup and a shaft-mounted gear.

Instrumentation

Turbine performance was determined by measurements taken at stations 2 and 4; and overall performance, which includes the diffuser and exit collector, was determined by measurements taken at stations 2 and 6. (See fig. 5 for station locations.) Turbine-inlet total temperature was taken at station 1 and was assumed to be the same at station 2. Thermocouple rakes could not be installed at station 2 because it would have involved drilling through several mating parts (see fig. 1). At station 1 the instrumentation consisted of four total-temperature rakes spaced at 90° intervals around the circumference. At stations 2 and 3 (stator inlet and exit) there were eight wall static-pressure taps with four each on the inner and outer walls. These inner and outer wall taps were located opposite each other at 90° intervals around the circumference. At station 4, approximately one rotor mean diameter axial chord length downstream of the rotor trailing edge, the static pressure, total pressure, total temperature, and flow angle were measured. The static pressure was measured with eight wall taps with four each on the inner and outer walls. These inner and outer wall taps were located opposite each other at 90° intervals around the circumference. Three

self-alining claw type probes were located 90° apart. These self-alining probes were used for the measurement of rotor-exit total pressure, total temperature, and flow angle. A photograph and description of this probe-actuator system are given in reference 3. During performance tests, the probes were set at radial distances to measure at area center radii of three equal annular areas. The self-alining probes were then used to obtain the radial distribution of rotor-exit total pressure, total temperature, and flow angle at design equivalent speed and design equivalent power. Two static-pressure taps were installed at station 5 near the exit of the diffuser, one on the inner and one on the outer wall. These were used in determining the pressure recovery of the diffuser. At station 6 there were four static-pressure taps located 90° apart circumferentially. These could be used as total-pressure measurements since the velocity in the exit collector was essentially zero. In addition, there were wall static-pressure taps located along the outer and inner walls of the diffuser to determine the variation of static pressure through the diffuser.

Absolute pressures at the various stations were measured directly with absolute pressure transducers. The data were recorded by integrating digital equipment.

Procedure

Performance data were taken at nominal stator-inlet total conditions of 303 K and 0.42 bar. These conditions give a Reynolds number that is the same as that for engine operating conditions. Data were obtained over a range of stator-inlet-total- to rotor-exit-static-pressure ratio of about 1.11 to 2.45 and a speed range from 0 to 130 percent of design.

Friction torque of the bearings, seals, and coupling windage was obtained by measuring the amount of torque required to rotate the shaft over the range of speeds covered in the investigation. A friction torque value of 1.5 newton-meters, which is about 29 percent of the turbine torque at design equivalent speed and design equivalent power, was obtained at design speed. During the friction tests, axial thrust loads were applied on the turbine thrust bearing. The results indicated no measurable change in friction in the 0- to 222-newton thrust load in the range encountered in the performance tests. The friction torque was added to the dynamometer torque to obtain the turbine aerodynamic torque.

The turbine was rated on the basis of both total η' and static η efficiency. The total pressures at stations 2 and 4 were calculated from mass flow, static pressure, total temperature, and flow angle from the following equation:

$$p' = p\left\{\frac{1}{2} + \frac{1}{2}\left[1 + \frac{2(\gamma - 1)R}{\gamma}\left(\frac{w\sqrt{T'}}{pA\cos\alpha}\right)^2\right]^{1/2}\right\}^{\gamma/(\gamma-1)}$$

RESULTS AND DISCUSSION

This section gives the performance of the turbine, blading, exit diffuser, and exit collector. Internal flow characteristics are also given in terms of static-pressure variations through the turbine and the velocity diagrams at design equivalent power as determined by the radial surveys of rotor-exit total pressure, total temperature, and flow angle. Included is a discussion of the performance of the exit diffuser in terms of the pressure-recovery coefficient.

Turbine Performance

Equivalent torque. - Figure 6 shows the variation of equivalent torque with stator-inlet-total- to rotor-exit-static-pressure ratio for lines of constant speed. An equivalent torque of about 16.20 newton-meters was obtained at design equivalent speed and an equivalent total- to static-pressure ratio p'_2/p_4 of 1.775. This was about 3 percent smaller than the design value of 16.70 newton-meters. This operating point corresponds to the overall design equivalent pressure ratio p'_2/p'_6 of 1.698. Zero speed torque was about 32.4 newton-meters at the total- to static-pressure ratio of 1.775. Thus zero speed torque was twice that obtained at design equivalent speed. The figure also shows that limiting loading was not reached for the range of pressure ratio investigated.

Equivalent mass flow. - Figure 7 shows the variation of equivalent mass flow with stator-inlet-total- to rotor-exit-static-pressure ratio p'_2/p_4 for lines of constant speed. All speed lines were not plotted since large amounts of data were taken and there were small differences in mass flow for each change in speed at any given pressure ratio. The figure indicates the spread of the data and a choked stator for pressure ratios greater than 2.2.

The equivalent mass flow was about 1.014 kilograms per second at design equivalent speed and at $p'_2/p'_6 = 1.698$. This is about 5.7 percent smaller than the design value of 1.075 kilograms per second. The comparison of engine equivalent mass flow and the test rig equivalent mass flow must take into consideration that engine hardware

was used and that the turbine operated at cold conditions. The difference in thermal expansion under these two conditions would increase the turbine flow area in the engine by about 2 percent. Therefore, the equivalent flow rate, for the component tests, would be about 2 percent lower than that obtained with engine operation. Therefore, the measured equivalent mass flow was about 3.7 percent smaller than the design value. This difference in mass flow could be primarily due to the accuracy in setting the design stator blade chord angle and to stator losses being greater than design. A 1^{o} error in setting angle would result in a change in mass flow of about 5 percent. The combination of a torque value, which is about 3 percent smaller than design, and a mass flow, which is 5.7 percent smaller than design, will result in the overall turbine efficiency being about 2 points higher than the design value of 0.742.

Performance maps. - The performance maps of figure 8 were obtained from crossplots, computed from values selected from smoothed curves of equivalent torque and mass flow. The performance map shows equivalent power as a function of the mass-flow - speed parameter with lines of constant equivalent speed. Lines of constant pressure ratio and efficiency are superimposed. Figure 8(a) shows the performance in terms of total conditions at the stator inlet and the rotor exit. At equivalent design speed and design equivalent power of 32.3 kilowatts, the total efficiency was slightly above 0.77. Over the range of pressure ratio and speed investigated, the total efficiency varied from 0.55 at the 30-percent speed line to above 0.79 at speeds from 110 to 130 percent and pressure ratios of about 2.0 and greater. Figure 8(b) shows performance map based on stator-inlet-total- to rotor-exit-static-pressure ratio. At the condition corresponding to design speed and equivalent power, the efficiency was about 0.70. Since the total efficiency was about 0.77 for this same operating point, there were about 7 points in efficiency due to rotor exit kinetic energy.

Over the range of pressure ratio and speeds investigated, the static efficiency varied from 0.45 at the 30-percent speed line to slightly over 0.71 at speeds of from 110 to 130 percent and pressure ratios of 2.1 and greater.

Figure 8(c) shows the overall performance (turbine and exit diffuser) in terms of total conditions. At design speed and design equivalent power the total efficiency was slightly over 0.76. This is about 2 points higher than the design value of 0.742. The static efficiency at this operating point was also slightly over 0.76. Therefore, there was about 1-point drop in total efficiency and a 6-point increase in static efficiency through the diffuser and the exit collector. Comparison of this operating point with that of figure 8(b) indicates that 85.7 percent of the rotor kinetic energy was recovered by the diffuser and the exit collector.

Over the range of pressure ratio and speed investigated, the overall total efficiency varied from about 0.55 at a pressure ratio of 1.3 and 30 percent speed to

0.76 over a comparatively wide range of speeds (80 to 130 percent) and pressure ratios (1.4 to 2.20).

Internal Flow Characteristics

Static pressure through turbine. - Figure 9 shows the variation of the static pressure through the turbine for operation at design equivalent speed and over a range of rotor-exit-static- to stator-inlet-total-pressure ratios. Variations of static pressure through the turbine at the outer wall is shown in figure 9(a). Since the rotor passage is not choked, stator and rotor reaction increased with decreasing rotor-exit static pressure. Figure 9(b) shows the static-pressure variations along the inner wall. The figure shows that there was negative reaction across the rotor for all pressure ratios investigated. This could result in flow separation along the rotor blade hub.

Rotor-exit total pressure and flow angle. - Figure 10(a) shows the radial variation of rotor-exit total pressure for operation at design equivalent speed and design equivalent power. The difference between the total and static pressures indicates lower velocities at the inner wall than at midspan. As will be discussed in the next section, this may be the result of high blade-profile losses and possible flow separation due to high negative reaction and high incidence at the rotor hub region.

Figure 10(b) shows the radial variation of rotor-exit absolute flow angle. Positive angles indicate a negative contribution to specific work. The combination of larger flow angles at the inner wall, or hub, region with lower velocities suggests that the mass flow was therefore lower along this region than along the rest of the passage height. This would also indicate that the losses were also large along the hub, or inner wall, region.

Velocity diagrams. - Figure 11 shows the velocity diagrams for the hub, mean, and tip or outer wall sections. The diagrams were calculated from radial surveys at the rotor exit of total pressure, total temperature, and flow angle. The radial variation of specific work was determined from measurements using the measured turbine-inlet total temperature, which was assumed constant from the inner to outer wall and the measured radial variation of rotor-exit total temperature. The rotor-exit total temperature was adjusted by a constant value from hub to outer wall so that the mass-average specific work as determined from temperature measurements was the same as that determined from torque, mass flow, and speed measurements. Rotor-exit absolute velocity and whirl velocities for each radial position were determined by the total pressure, static pressure, and flow angle. A linear variation in static pressure was assumed from the hub and outer wall static-pressure values. At the stator exit, the whirl velocity was determined from specific work, wheel speed, and the rotor-exit whirl velocity. The stator-exit absolute velocities were calculated from the assumed

linear variation in static pressure and a stator total-pressure loss of 3 percent. The stator-exit flow angle was determined by the whirl and resultant velocities. Mass flow was integrated from inner to outer wall. The assumed total-pressure loss was adjusted until the integrated mass flow was the same as that determined by measurements with the thin-plate orifice.

The velocity diagram of figure 11 shows that there was negative reaction along the rotor hub region. The calculated rotor reactions were - 0.160, 0.195, and 0.339 for the hub, mean, and tip sections. Reference 4 indicates that, for an ideal rectangular form of loading diagram, negative reaction results in increased total blade-surface diffusion. Increased total blade-surface diffusion will result in high blade-profile loss. The high negative reaction at the rotor may also have resulted in flow separation.

Rotor incidence angles were -15.1°, $+4.8^{\circ}$, and -3.6° at the hub, mean, and tip sections. Based on the results of Ainley and Mathieson (ref. 5), this high negative rotor incidence at the hub section could result in about a 30-percent increase in blade-profile loss, when compared with that obtained at the optimum incidence value. Therefore, the high incidence and high negative reaction will result in excessive blade profile losses with possible flow separation at the hub section.

The stator-exit deviation angles were $+10.0^{\circ}$, -0.3°, and $+3.4^{\circ}$ for the hub, mean, and tip sections, respectively. The underturning of the flow at the hub and tip sections can be the result of leakage at the ends of the blade due to the end clearances. The larger deviation at the stator hub than at the tip may be the result of the larger end clearance at the stator hub, or inner wall.

The rotor-exit deviation angles were -17.6°, $+6.6^{\circ}$, and $+4.7^{\circ}$ for the hub, mean, and tip sections, respectively. The high amount of overturning suggests a strong passage vortex at the rotor hub region. The absence of overturning at the rotor tip or outer wall could result from the interaction of rotor tip leakage counteracting the effect of a passage vortex on the flow.

The velocity diagram also indicates low mass flow along the hub, or inner wall, at the rotor exit. This may be the result of the combined effect of high incidence angle and high negative reaction causing high total-pressure loss, which would allow secondary flows to develop. Subsonic flow occurred through all sections of the stator and rotor. These subsonic velocities therefore indicate that the stator or rotor was not choked at design equivalent speed and design equivalent work.

Diffuser Performance

As mentioned in the performance section of the report, there was about 1-point decrease in total efficiency through the diffuser and exit collector for operation at

design equivalent speed and design equivalent work. At this operating condition, the diffuser static-pressure-recovery coefficient was 0.28. The recovery coefficient is defined as the static-pressure rise divided by the diffuser-inlet velocity head. The static-pressure-recovery coefficient of the diffuser and exit collector was 0.54. Therefore, the static-pressure recovery in the diffuser was about 52 percent of the total recovered by the diffuser and exit collector. The overall diffuser effectiveness e, which relates the actual pressure rise to that achievable from the same geometry with ideal, one-dimensional flow at the same flow rate, was 0.36. Based on the results of reference 6 a pressure recovery of about 0.30 would be expected for the given diffuser-area ratio and diffuser-average-surface-length-to-inlet-annulus-height ratio. Improved pressure recovery and effectiveness, with the given area ratio, could be obtained if the diffuser-average-surface-length-to-inlet-annulus-height ratio was increased from the present value of 3.13 to about 5.0. With this increase in diffuser average surface length, a diffuser overall effectiveness of about 0.76 could be obtained. This would result in about a 3-point increase in static efficiency over the present value of 0.725 based on stator-inlet to diffuser-exit conditions. This improvement may not be reflected in a significant increase in overall efficiency based on stator-inlet to -exit collector conditions.

Figure 12 shows the diffuser-outer- and inner-wall local-static-to-total-pressure-ratio variation as a function of percent of axial surface length. The figure shows that a greater static-pressure rise occurs along the outer wall than along the inner wall. This was to be expected since the velocity diagram indicated low velocity at the rotor hub, or inner wall.

SUMMARY OF RESULTS

An experimental investigation was conducted on the baseline power turbine which was designed for a 112-kilowatt gas-turbine engine. Cold-air tests were made for the 100-percent power-point setting angle of the variable stator. Results of this investigation at design equivalent speed and design equivalent power may be summarized as follows:

1. An equivalent mass flow of 1.014 kilograms per second was obtained at design equivalent speed and design equivalent overall total-pressure ratio (1.698). This equivalent mass flow is about 5.7 percent smaller than design value. Because engine hardware was used for the investigation, the turbine was tested with cold dimensions. Thermal expansion at design turbine-inlet temperature would increase the turbine flow area by about 2 percent. Therefore, the equivalent mass flow for the component tests would be about 2 percent less than that obtained with engine operation.

2. The total efficiency based on stator-inlet-to-rotor-exit conditions was slightly above 0.77 at design equivalent speed and design equivalent power. The static efficiency for this same operating condition was slightly above 0.70. Therefore, about 7 points in efficiency were due to rotor-exit kinetic energy.

3. The total and static efficiency based on stator-inlet to exit-collector conditions, was slightly over 0.76. This is about 2 points higher than the design value of 0.742. Thus the diffuser and exit collector recovered about 85.7 percent of the rotor-exit kinetic energy.

4. There was about 1-point drop in total efficiency and a 6-point increase in static efficiency through the diffuser and exit collector.

5. The diffuser static-pressure-recovery coefficient was 0.28, which was about 52 percent of that recovered by the diffuser and exit collector. The overall diffuser effectiveness was 0.36. If the diffuser-average-surface-length-to-inlet-annulus-height ratio was increased from 3.13 to 5.0, the overall effectiveness could be increased to a value of about 0.76. This would result in about a 3-point increase in static efficiency over the present value of 0.725 based on stator-inlet to diffuser-exit conditions. This improvement in efficiency may not be reflected in a significant increase in overall efficiency based on stator-inlet to exit-collector conditions.

6. Velocity diagrams were calculated from radial surveys at the rotor exit. The rotor reactions were -0.160, 0.195, and 0.339 for the hub, mean, and tip sections. The rotor incidence angles were -15.1°, $+4.8^{\circ}$, and -3.6° at the hub, mean, and tip sections. The high negative reaction and high negative incidence at the rotor hub section results in excessive blade profile losses with possible flow separation.

Lewis Research Center,
National Aeronautics and Space Administration,
Cleveland, Ohio, April 22, 1977,
778-32.

REFERENCES

1. Angell, P. R.; and Golec, T.: Upgrading Automotive Gas Turbine Technology. An Experimental Evaluation of Improvement Concepts. SAE Paper 760280, Feb. 1976.

2. Meng, Phillip R.; and Wulf, Richard F.: Experimentally-Determined External Heat Loss of Automotive Gas Turbine Engine - Preliminary Data Report. NASA TM X-71709, 1975.

3. Futral, Samuel F.; Kofskey, Milton G.; and Rohlik, Harold E.: Instrumentation Used to Define Performance of Small Size, Low Power Gas Turbines. NASA TM X-52522, 1969.

4. Stewart, Warner L.; Whitney, Warren J.; and Wong, Robert Y.: A Study of Boundary-Layer Characteristics of Turbomachine Blade Rows and Their Relation to Over-All Blade Loss. J. Basic Eng., vol. 82, Sept. 1960, pp. 588-592.

5. Ainley, D. G.; and Mathieson, G. C. R.: Examination of the Flow and Pressure Losses in Blade Rows of Axial-Flow Turbines. Rept. 86. Nat. Gas Turbine Establishment, 1953.

6. Sovran, Gino; and Klomp, Edward D.: Experimentally Determined Geometries for Rectilinear Diffusers with Rectangular, Conical, or Annular Cross Section. Fluid Mechanics of Internal Flow, Gino Sovran, ed., Elsevier Publishing Co., 1967, pp. 270-307.

TABLE I. - TURBINE DESIGN POINT PARAMETERS

Parameter	Engine operation	Equivalent conditions
Inlet temperature, K	1104.2	288.2
Inlet pressure, bar	1.894	1.01
Mass flow, kg/sec	1.001	1.075
Rotative speed, rpm	35 845	18 534
Specific work, Δh, J/g	112.5	30.2
Mean rotor tip diameter, D_m	16.511	16.511
Work factor, $\Delta V_u/U_m$	1.172	1.172
Total efficiency (including diffuser), η	0.742	0.742
Total pressure ratio (including diffuser)	1.661	1.698
Power, kW	112.5	32.3

TABLE II. - TURBINE BLADING PARAMETERS

Blade row	Section	Solidity, σ	Aspect ratio,[a] $\mathcal{A}$	Reaction,[a] R_x	Number of blades	Tip clearance, cm
Stator	Hub	1.49	-----	-----	27	0.041
	Mean	1.53	0.839	-----	--	-----
	Tip	1.56	-----	-----	--	.025
Rotor	Hub	1.98	-----	-0.160	51	-----
	Mean	1.65	1.486	.195	--	-----
	Tip	1.44	-----	.339	--	0.046

[a]See SYMBOLS for definition.

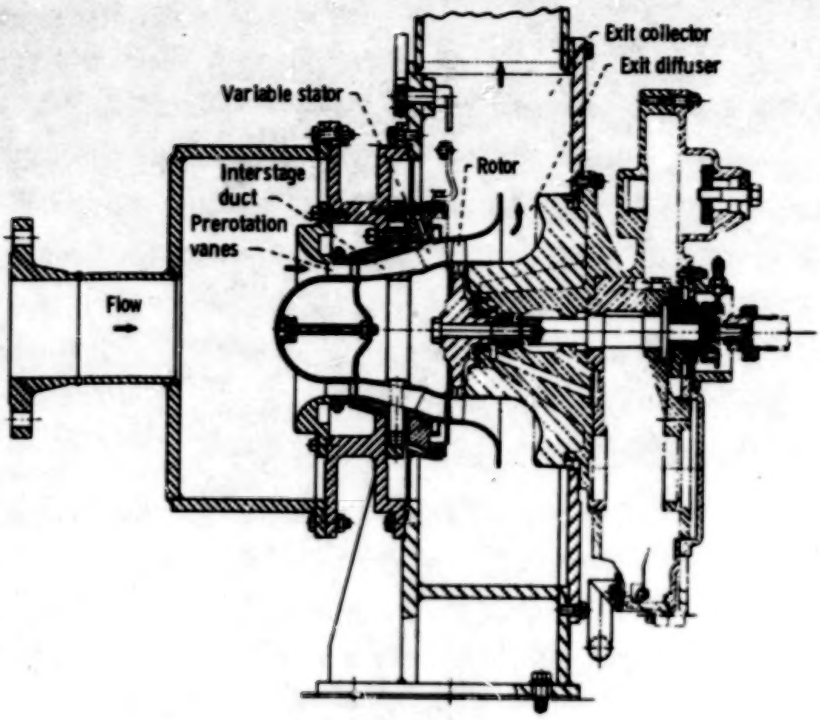

Figure 1. - Schematic of turbine for tests.

Figure 2. - Variable stator assembly.

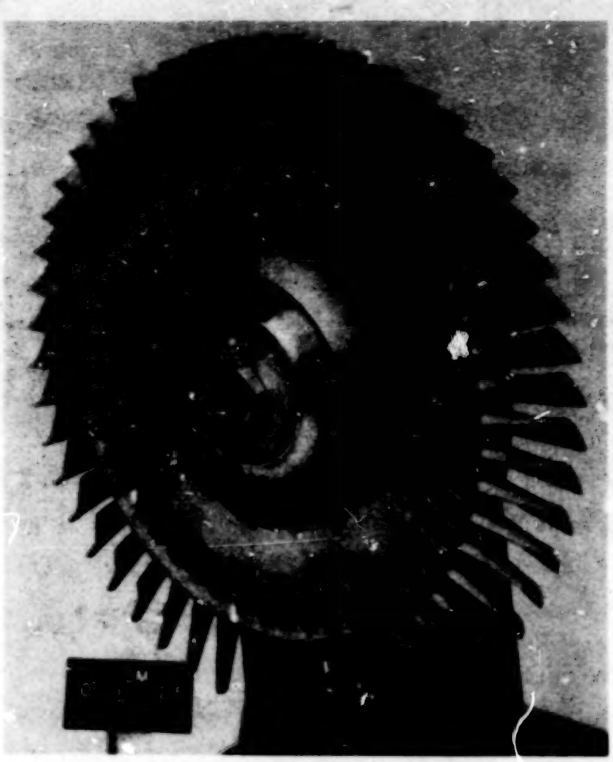

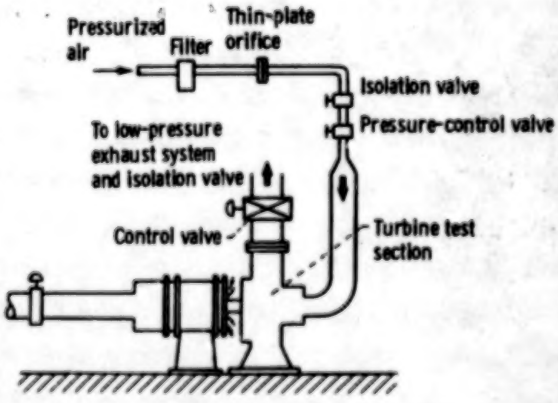

(a) Schematic of piping and test equipment.

(b) Turbine test apparatus.

Figure 4. - Experimental equipment.

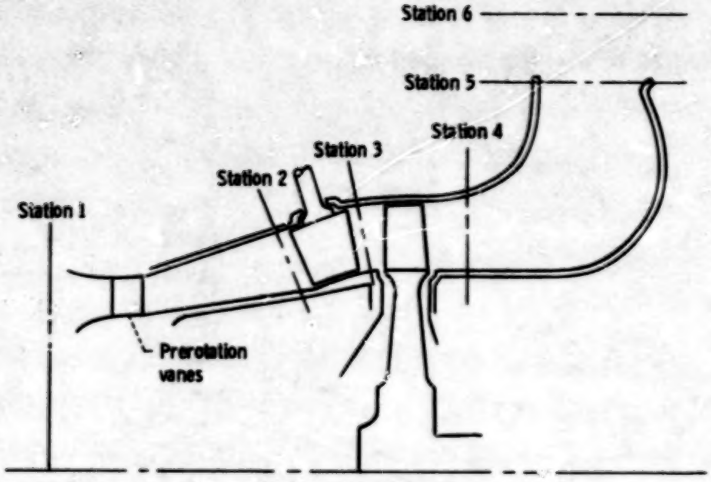

(a) Measuring stations.

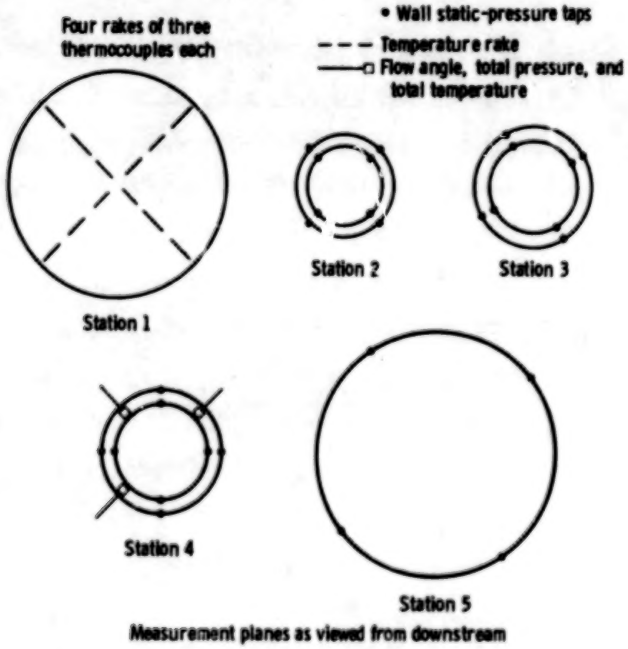

Measurement planes as viewed from downstream

(b) Research instrumentation.

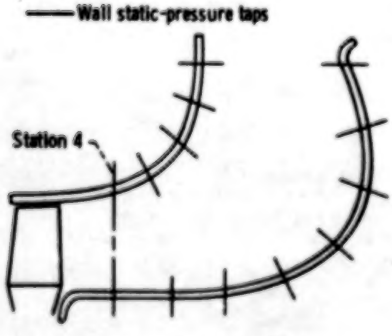

(c) Diffuser instrumentation.

Figure 5. - Instrumentation.

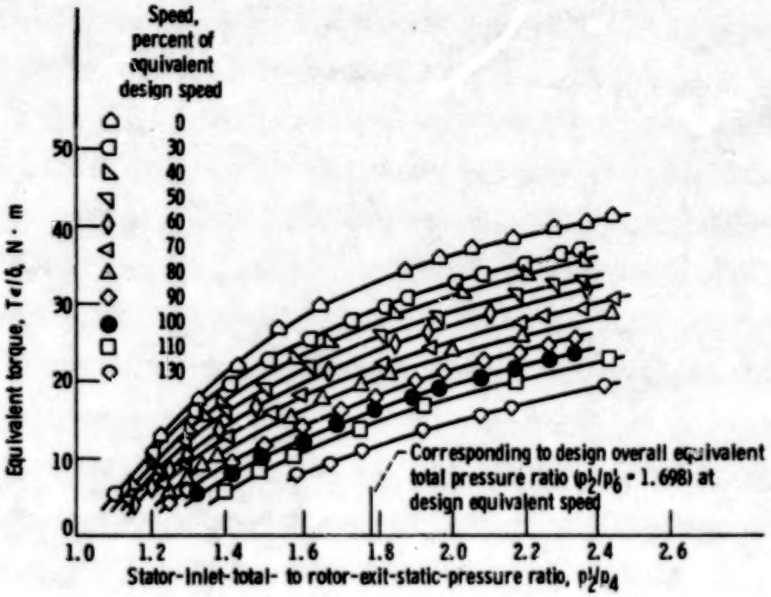

Figure 6. - Variation of torque with pressure ratio and speed.

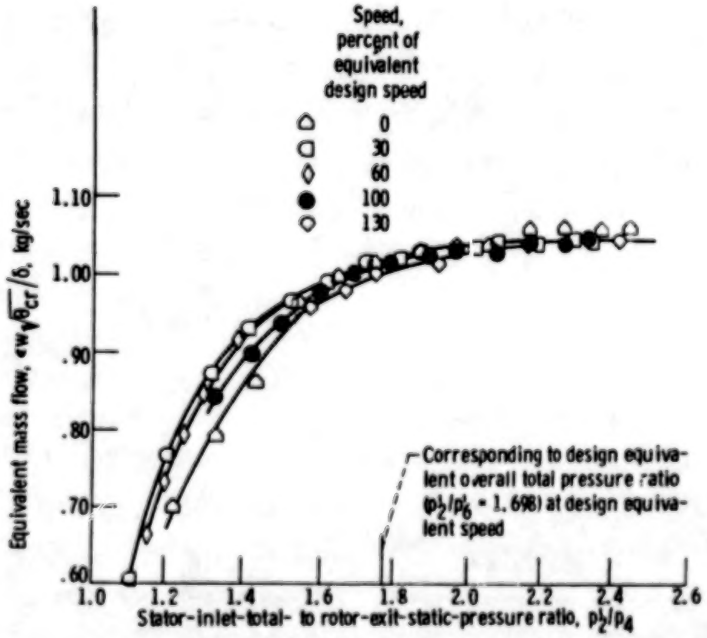
Speed, percent of equivalent design speed
0
30
60
100
130
Equivalent mass flow, $\epsilon w_4\sqrt{\theta_{cr}}/\delta$, kg/sec
Corresponding to design equivalent overall total pressure ratio (p_2'/p_6' = 1.698) at design equivalent speed
Stator-inlet-total- to rotor-exit-static-pressure ratio, p_2'/p_4

Figure 7. - Variation of mass flow with pressure ratio and speed.

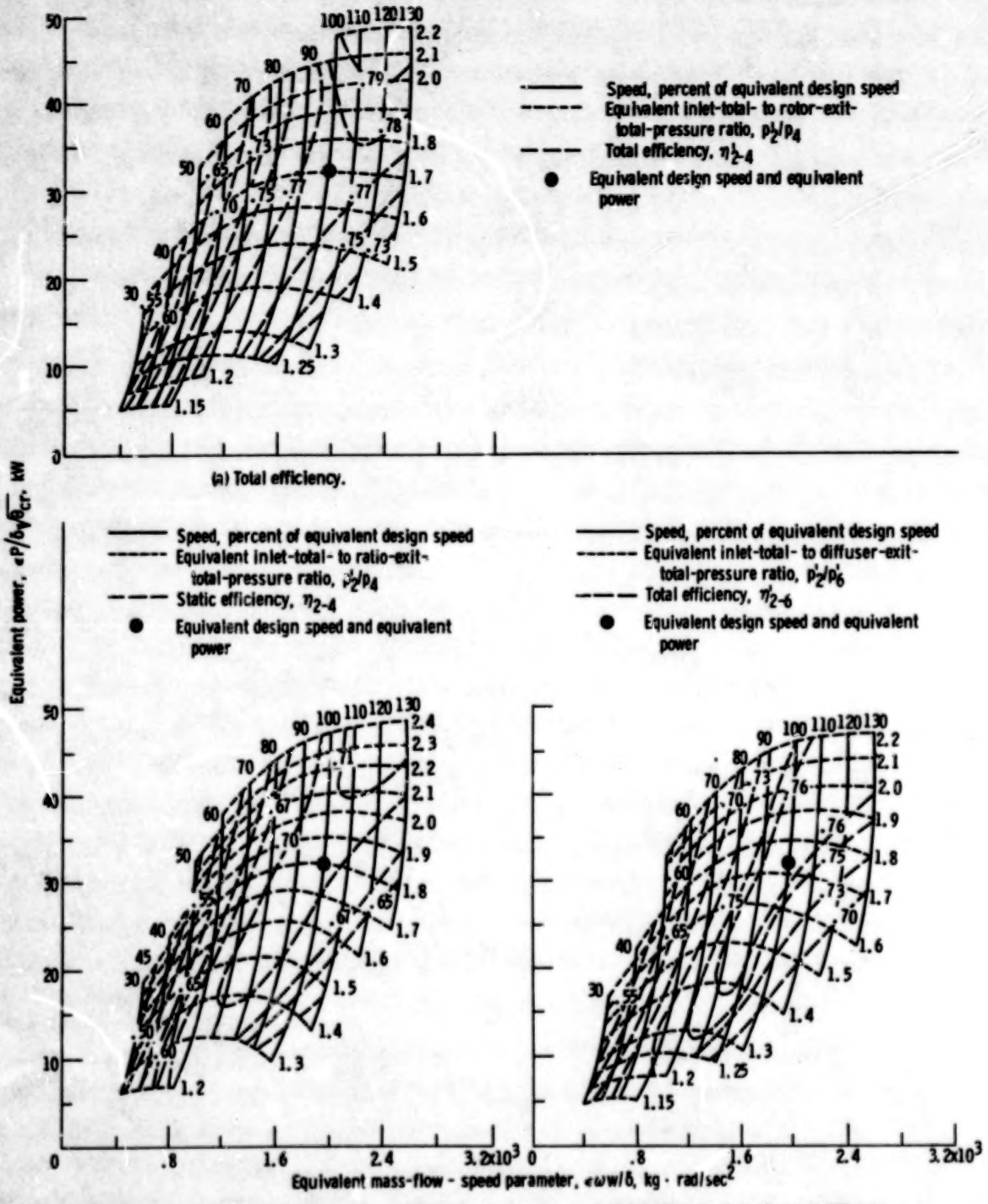
Speed, percent of equivalent design speed
Equivalent inlet-total- to rotor-exit-total-pressure ratio, p_2'/p_4
Total efficiency, η_{2-4}'
Equivalent design speed and equivalent power
Speed, percent of equivalent design speed
Equivalent inlet-total- to ratio-exit-total-pressure ratio, p_2'/p_4
Static efficiency, η_{2-4}
Equivalent design speed and equivalent power
Speed, percent of equivalent design speed
Equivalent inlet-total- to diffuser-exit-total-pressure ratio, p_2'/p_6'
Total efficiency, η_{2-6}'
Equivalent design speed and equivalent power
Equivalent power, $\alpha P/\delta\sqrt{\theta_{cr}}$, kW
Equivalent mass-flow - speed parameter, $\alpha\omega w/\delta$, kg · rad/sec^2

(a) Total efficiency.

(b) Static efficiency.

(c) Total efficiency including exit diffuser.

Figure 8. - Turbine performance map.

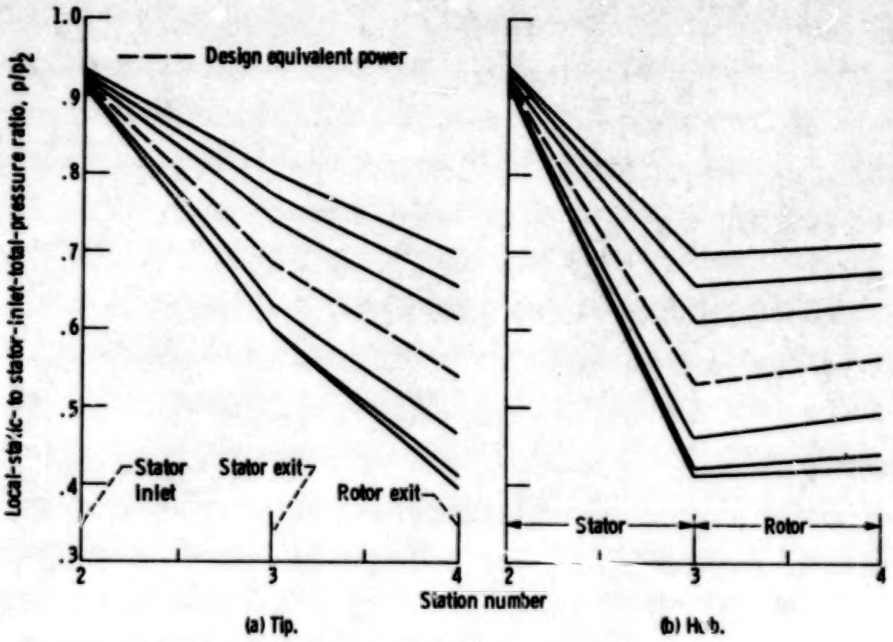

Figure 9. - Variation of local-static pressure through turbine at design speed and over range of stator-inlet-total- to rotor-exit-static-pressure ratios.

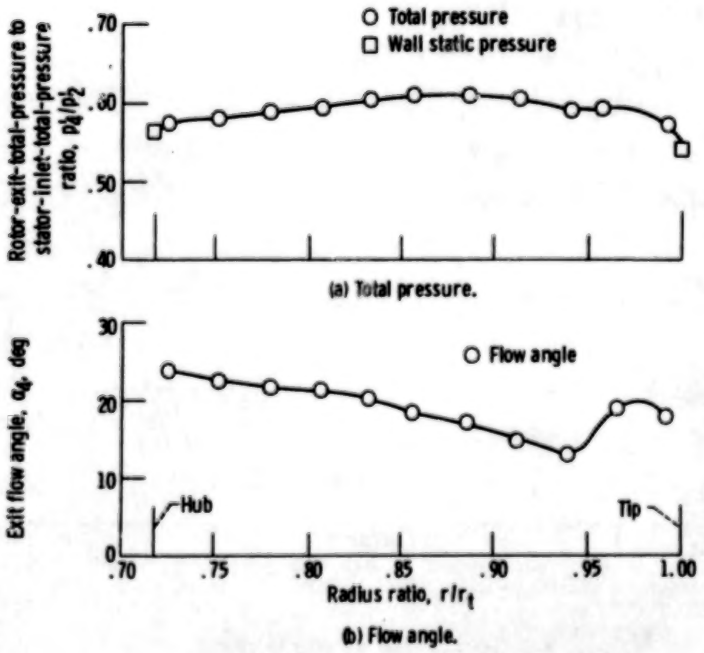

Figure 10. - Variation of rotor-exit total pressure and flow angle with radius ratio at design speed and design equivalent power.

Station:	Hub	Mean	Tip
2, stator inlet 3, stator exit, rotor inlet 4, rotor exit	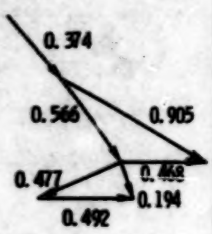	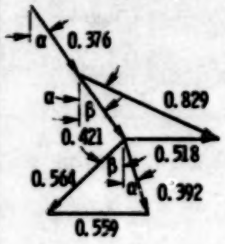	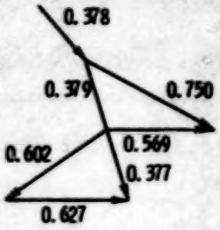
	Radius, cm		
Station 2 Station 3 Station 4	6.160 7.483 7.419	7.237 8.288 8.445	8.313 9.093 9.527
	Angle, deg		
α_2 α_3 β_3 α_4 β_4	39.5 61.7 37.5 22.6 66.8	43.5 67.5 38.0 18.5 49.3	40.2 61.8 14.6 19.5 54.7

Figure 11. - Velocity diagrams calculated from experimental results at design speed and design equivalent power.

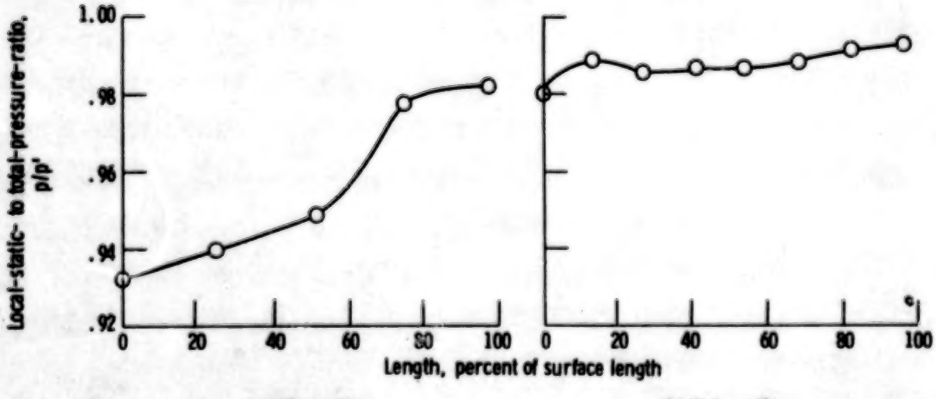

(a) Tip section. (b) Hub section.

Figure 12. - Variation of local-static- to total-pressure ratio through diffuser at design speed and design equivalent power.

1. Report No.	2. Government Accession No.	3. Recipient's Catalog No.
NASA TP-1007		

4. Title and Subtitle	5. Report Date
COLD-AIR PERFORMANCE OF FREE-POWER TURBINE DESIGNED FOR 112-KILOWATT AUTOMOTIVE GAS-TURBINE ENGINE I - DESIGN STATOR-VANE-CHORD SETTING ANGLE OF 35°	January 1978
	6. Performing Organization Code
7. Author(s)	8. Performing Organization Report No.
Milton G. Kofskey and William J. Nusbaum	E-8964
	10. Work Unit No.
9. Performing Organization Name and Address	778-32
National Aeronautics and Space Administration Lewis Research Center Cleveland, Ohio 44135	11. Contract or Grant No.
	13. Type of Report and Period Covered
12. Sponsoring Agency Name and Address	Technical Paper
National Aeronautics and Space Administration and Department of Energy Washington, D.C. 20545	14. Sponsoring Agency Code Report No.
	CONS/1011-12

15. Supplementary Notes

This work was a joint effort of NASA and the DOE Office of Conservation and Solar Applications, partly funded by DOE under Interagency Agreement EC-77-A-31-1011.

16. Abstract

A cold-air experimental investigation of a free-power turbine designed for a 112-kW automotive gas-turbine was made over a range of speeds from 0 to 130 percent of design equivalent speeds and over a range of pressure ratio from 1.11 to 2.45. Results are presented in terms of equivalent power, torque, mass flow, and efficiency for the design power-point setting of the variable stator.

17. Key Words (Suggested by Author(s))	18. Distribution Statement
Turbine engines; Automobile engines; Axial flow turbines; Single stage turbines; Gas turbines	Unclassified - unlimited STAR Category 07 DOE Category UC-96

19. Security Classif. (of this report)	20. Security Classif. (of this page)	21. No. of Pages	22. Price*
Unclassified	Unclassified	22	A02

* For sale by the National Technical Information Service, Springfield, Virginia 22161

NASA-Langley, 1978